Shape and Non–Principal Axis Spin State of Asteroid 4179 Toutatis

R. Scott Hudson* and Steven J. Ostro

Radar observations of Toutatis placed hundreds to thousands of pixels per image on the asteroid and revealed it to be a non–principal axis rotator. The radar data are used to calculate Toutatis's three-dimensional shape, spin state, and the ratios of the principal moments of inertia. Toutatis is rotating in a long-axis mode characterized by periods of 5.41 days (rotation about the long axis) and 7.35 days (average for long-axis precession), and its dimensions along the principal axes are 1.92, 2.40, and 4.60 kilometers. To within the model's uncertainties, Toutatis's density is homogeneous, or its inhomogeneities mimic the inertia tensor of a homogeneous body.

Delay-Doppler radar is a unique ground-based source of fine-resolution images of Earth-orbit–crossing asteroids (ECAs). However, these images represent a nonintuitive projection and are subject to global aliasing. Consequently, optimal extraction of the information they contain requires their inversion with a comprehensive physical model. In this report we present an inversion of Toutatis images that yields the most detailed physical characterization of an ECA to date. Toutatis's unusual spin state and highly irregular shape raise perplexing questions about its origin and collisional history.

Our least-squares estimation of Toutatis's shape and spin state was made from 17 Goldstone "low-resolution" (0.5 μs by 0.1 Hz) images from 2 through 18 December 1992 and a single Arecibo (0.2 μs by 0.012 Hz) image from 19 December 1992 (*1*). We proceeded in a manner similar to that used for asteroid 4769 Castalia (*2*); however, the analysis was complicated by Toutatis's unusual rotation. For the vast majority of solar system objects, the spin vector **W** is constant and parallel to both the angular momentum vector **L** and the maximum-moment principal axis of inertia (the object's short axis). For such principal axis (PA) rotation, two constant angles θ and ϕ fix the direction of this rotation pole and another angle $\psi = (2\pi/P)t$, with P being the spin period, gives the rotation phase. These three Euler angles give the orientation of the body as a function of time t (*3*). For a non–principal axis (NPA) rotator like Toutatis, **W** is not parallel to **L** and is not constant in either body-fixed or inertial coordinates. Moreover, all three Euler angles are nonlinear functions of time. The spin vector **W** is periodic in a body-fixed frame but not in an inertial frame, and in general the object never repeats any particular inertial orientation.

Given principal moments of inertia $I_s \geq I_i \geq I_l$, where the subscripts refer to the short, intermediate, and long axes, an object's motion is fully determined by specifying at some time t_0 the initial conditions θ_0, ϕ_0, $\dot{\theta}_0$, and $\mathbf{W}_0$. Integration of Euler's equations then provides ϕ, θ, ψ, and **W** as functions of time (*3*). Because those equations depend on the moments of inertia only through the ratios I_s/I_l and I_i/I_l, a total of eight parameters is needed to specify a general spin state.

Initially, Toutatis was represented by 2.5- and 1.5-km spheres in contact. The Euler angles θ and ϕ oriented the z axis, through the sphere's centers, with respect to ecliptic coordinates as functions of time, and the Euler angle ψ gave the angular position of the body about this axis. For each frame, the orientation of this simple shape was estimated "by hand," with no consideration of the underlying dynamics, by observing the correspondence between observed and modeled data. Because of the shape's symmetry about the z axis, no constraints could be placed on the angle ψ, but this process did produce a series of coarse estimates for θ and ϕ in each frame. We then fit a spin state to these approximate θ and ϕ values using the inertia tensor of the two-sphere model in the integration of Euler's equations. The resultant, rather crude description of the rotation state provided adequate initial conditions for simultaneous least-squares estimation of the full set of parameters describing the asteroid's shape, radar scattering properties (*4*), and dynamics.

Our model defines Toutatis's shape (Fig. 1) by a set of vertices $\mathbf{v}_i$, $1 \leq i \leq 1600$, grouped into triples to define 3196 triangular surface facets (*5*) whose average area is $(84\ \text{m})^2$. The vertices parameterize the shape as a deformed ellipsoid by means of $\mathbf{v}_i = \mathbf{a}_i + r_i\,\mathbf{u}_i$, where $\mathbf{a}_i$ and $\mathbf{u}_i$ are points on, and the corresponding surface normals of, the dynamically equivalent, equal-volume ellipsoid (DEEVE), that is, the homogeneous ellipsoid that has the same moment ratios and volume as the asteroid. The parameters r_i specify Toutatis's topography in terms of its deviation from the DEEVE.

The shape and spin-state parameters were adjusted to minimize an objective function that was the sum of a least-squares goodness-of-fit measure (χ^2) and weighted penalty functions. The latter consisted of dynamical penalties and a concavity penalty. The dynamical penalties allowed control of the degree to which all the parameters were consistent with a hypothesis of uniform density. The concavity penalty suppressed topography not strongly required by the data.

The DEEVE has overall dimensions (1.70, 2.03, and 4.26) ± 0.08 km (*6*). These define Toutatis's dynamical elongations as 4.26/1.70 = 2.51 ± 0.16 and 4.26/2.03 = 2.10 ± 0.12. The maximum extents of the asteroid's shape along the principal axes, (1.92, 2.29, and 4.60) ± 0.10 km, define physical elongations (*7*) of 4.60/1.92 = 2.40

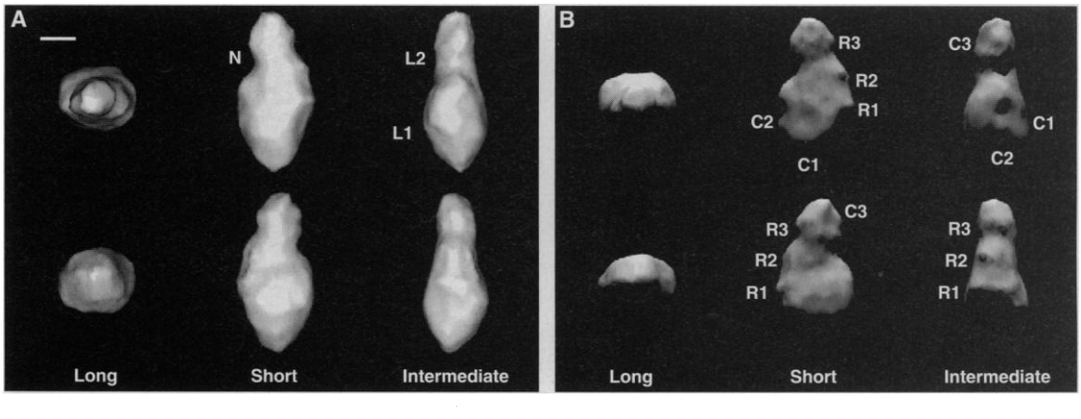

Fig. 1. (**A**) Renderings of the Toutatis model from both directions on the long, short, and intermediates axes. The bar at the upper left is 1 km long. Labels denote surface features discussed in the text. Source and observer are collocated. (**B**) Same as (A) but the source of illumination is moved 75° toward the top of the page. Lambertian scattering was used in all renderings. Features: L, lobe; N, neck; C, concavity; and R, ridge.

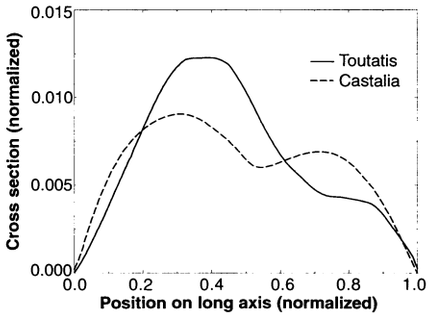

Fig. 2. Cross-sectional area versus position on the long axis for the Toutatis model and the lower-bound Castalia model (*2*). For comparison, both models were normalized to unit volume and unit long-axis length. Given uniform density, the curves would also correspond to mass distribution.

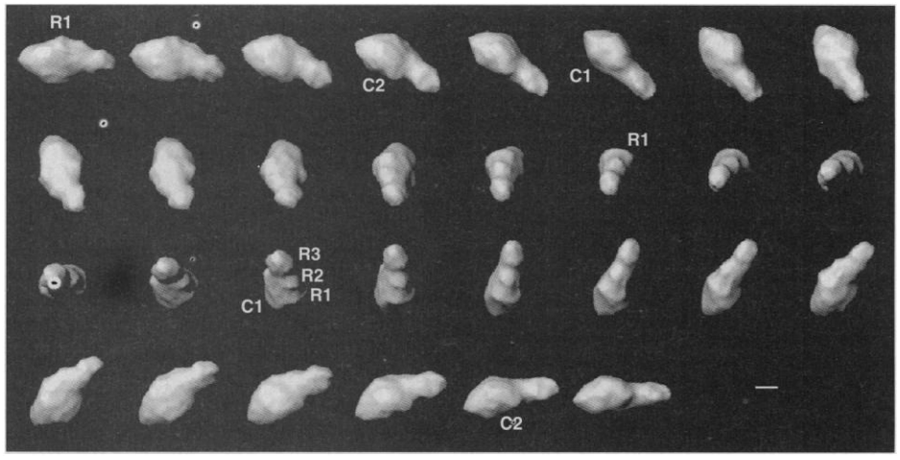

Fig. 3. Toutatis's shape and spin state rendered at 6-hour intervals beginning 3 December 1992, 18:00 UTC, and increasing left to right, top to bottom. Each row spans 2 days and the total sequence covers 7.25 days. The bar at the lower right is 1 km long. The view is looking south along the ecliptic pole with the vernal equinox to the right. An artificial light source is located 45° counterclockwise from the top and 60° out of the page. The angular momentum vector is to the left and 52° into the page. The long axis moves from being nearly in the plane of the ecliptic to nearly perpendicular to it, and the long-axis orientation (θ, ϕ) almost repeats after the 7.25 days (*8*). However, the orientation of the body about the long axis (ψ) is quite different between the beginning and end of this sequence, demonstrating that the complete motion of the object is not periodic. The labels corresponds to features in Fig. 1.

$\pm$ 0.18 and 4.60/2.29 = 2.01 $\pm$ 0.13.

Toutatis radar images appear bifurcated in every frame (*1*). Indeed, the intermediate- and short-axis views of Fig. 1A lead us to perceive the shape as consisting of two lobes, which we label L1 and L2; however, the asteroid's volume distribution along the long axis is not bimodal (Fig. 2). The most prominent features at the several-hundred-meter scale include the concavities labeled C1, C2, and C3 in Fig. 1B. Concavities C1 and C2 are the most circular, and we identify these as impact craters. Their close proximity and similar diameters (about 750 m) are intriguing. Concavity C3, which extends over most of the length of L2, is less circular but also may be an impact structure. The pattern of ridges R1, R2, and R3 dominates the relief in some views. The largest of these, R1, extends about 1 km across L1 and is oriented nearly normal to the asteroid's long axis. This is followed by a shorter ridge, R2, closer to L2. Feature R3 appears, in some views, to be an extension of the structure R1-R2. The 500-m-deep "neck" N extends part way around the opposite side of the asteroid from the structure R1-R2-R3, demarcating L1 and L2 in many views.

Toutatis's rotation (Fig. 3) is specified by the following initial conditions. The moment ratios are within 3% of I_3/I_1 = 3.19 and I_2/I_1 = 3.01. At t_0 = 11 December 1992, 9:21 UTC, the Euler angles of the principal axes of inertia with respect to ecliptic coordinates were within 3° of ϕ_0 = –103°, θ_0 = 94°, and ψ_0 = –136°, and the projection of $\mathbf{W}_0$ along the (short, intermediate, long) principal axes was within 1° day^{-1} of (20°, 32°, 98°) day^{-1}. These eight parameters define the direction of **L** as ecliptic longitude 180°, latitude –52°. The fact that $L^2/2EI_1$ = 0.55 (E is the rotational kinetic energy) is less than unity identifies the spin state (*3*) as a "long-axis mode." In body-fixed coordinates, **W** rotates about the long axis every P_1 = 5.41 days, and the complete motion consists of nonlinear periodic variations every P_1 days superposed on a uniform rotation about **L** every P_2 = 7.35 days (*8*).

The delay-Doppler projection is invariant with respect to rotation of the shape and spin state about the radar line of sight; however, plane-of-sky (POS) motion can break this ambiguity. For Toutatis, the POS motion was more than 100° during the 18 days of radar observations, and the solution is sensitive to all spin-state parameters. Moreover, independent confirmation of the model's prediction of the asteroid's POS orientation is available from two sources, as follows.

On 17 December 1992 at about 7:25 UTC, de Pater *et al.* (*9*) conducted radar aperture–synthesis observations of Toutatis, transmitting from Goldstone and receiving echoes at the Very Large Array (VLA). Although the resolution of 0.2 arc sec, equivalent to 10 km at the asteroid, did not resolve the object, an elongation at a position angle of about –61° was revealed in the difference between the image and a point source model. Figure 4A shows our model's prediction for Toutatis's orientation during the time of this observation; the line running through the model is the Goldstone-VLA prediction. This observation was fortunate to catch Toutatis at a time when its long axis was nearly parallel to the plane of the sky.

On 10 December 1992 at about 18:40 UTC, when the sun-Toutatis-Earth angle was about 90°, Noll *et al.* (*10*) imaged Toutatis with the Hubble Space Telescope (HST). The image pixels subtended 926 m on the asteroid (0.0439 arc sec), and the full width at half maximum of the core of the point spread function was 0.070 arc sec, corresponding to a resolution of 1.48 km at Toutatis. Figure 4B shows our predicted appearance of Toutatis, and Fig. 4C shows the same view with a pixel size of 453 m for comparison with figure 4 of (*10*). The ren-

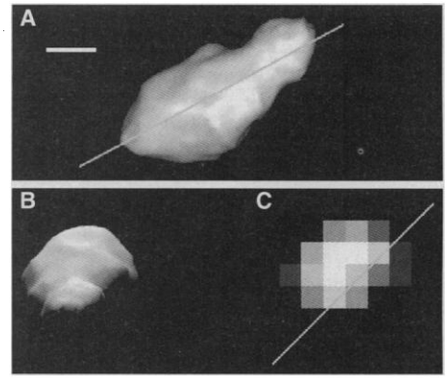

Fig. 4. (**A**) Toutatis model at 17 December 1992, 7:25 UTC, with zero-phase illumination. North is up. The line passes through the center of mass and is the Goldstone-VLA prediction (*9*) of Toutatis's elongation at that time. (**B**) Toutatis model at 10 December 1992, 18:40 UTC, with solar illumination. North is 112.8° clockwise from up. (**C**) Same as (B) but with 453-m pixels (*10*). The line passes through the center of mass at an angle of 45°.

R. S. Hudson, School of Electrical Engineering and Computer Science, Washington State University, Pullman, WA 99164–2752, USA.
S. J. Ostro, Jet Propulsion Laboratory, California Institute of Technology, Pasadena, CA 91109–8099, USA.
*To whom correspondence should be addressed.

dered model, with a maximum dimension of 2.2 km, is consistent with those authors' statement that the illuminated, visible area had a maximum size "most likely in the range from 1.7 to 2.4 km." Noll *et al.* also interpreted the HST data as suggesting an "extended feature at an angle of about 45° off the solar vector," which is indicated by the line in Fig. 4C. This apparent elongation was the result of the unusual shape of Toutatis and shadowing effects arising from the large illumination angle.

All of Toutatis's surface was observed in the 18-day sequence of images (*11*), and because of the NPA rotation, the entire inertia tensor can be determined to within a constant factor. The dynamical penalties that forced the shape and inertia tensor toward mutual consistency with uniform density were exerting negligible pressure on the best-fit solution; removing them led to no significant change in the model. That is, the model requires either that Toutatis is nearly homogeneous or that its inhomogeneities mimic the inertia tensor of a homogeneous body (*12*).

The source of Toutatis's topographic bifurcation is a mystery. Might feature N have been sculpted by a single direct impact or a sequence of impacts? Or is Toutatis a contact binary formed in a gentle collision between L1 and L2? One would also like to decipher the collisional history responsible for the R1-R2-R3 structure, as well as implications of the global topography at all perceptible scales for the object's internal configuration, for example, its cohesiveness (*13*). One is especially interested in how and when Toutatis was excited into such a slow, NPA rotation state (*14*). Collisional simulations (*15*) using our physical model may suggest answers to these questions.

REFERENCES AND NOTES

1. S. J. Ostro *et al.*, *Science* **270**, 80 (1995).
2. R. S. Hudson and S. J. Ostro, *ibid.* **263**, 940 (1994).
3. L. D. Landau and E. M. Lifshitz, *Mechanics* (Pergamon, New York, 1976); N. H. Samarasinha and M. F. A'Hearn, *Icarus* **93**, 194 (1991); M. J. S. Belton, W. H. Julian, A. J. Anderson, B. E. A. Mueller, *ibid.*, p. 183.
4. The differential radar cross section of the surface was modeled as $\sigma_0 = \rho\cos^n i$ (*2*). The model yielded the value $n = 2.3 \pm 0.5$; $n = 2$ corresponds to Lambertian scattering, or a "perfectly rough" surface.
5. D. Hearn and M. P. Baker, *Computer Graphics* (Prentice Hall, Englewood Cliffs, NJ, ed. 2, 1994).
6. These define an effective diameter of 2.45 km. Thermal modeling by various researchers had suggested effective diameters between 2 and 3 km. D. J. Tholen, *Bull. Am. Astron. Soc.* **24**, 934 (1992); D. F. Lupishko, S. V. Vasilyev, J. S. Efimov, N. M. Shakhovskoj, *Icarus* **113**, 200 (1995).
7. S. J. Ostro *et al.*, *Nature* **375**, 474 (1995).
8. J. R. Spencer *et al.* [*Icarus*, in press] attempted to deduce the spin period of Toutatis from optical light curves. They found a best fit for $P = 7.25$ days but concluded from the poor fit that the rotation was more complex than PA.
9. I. de Pater *et al.*, *Icarus* **111**, 489 (1994).
10. K. S. Noll, H. A. Weaver, A. D. Storrs, B. Zellner, *ibid.* **113**, 353 (1995).
11. This was not apparent until the modeling was completed.
12. All detailed asteroid shape modeling to date has failed to find evidence for significant inhomogeneity (*2*); P. C. Thomas *et al.*, *Icarus* **107**, 23 (1994); P. C. Thomas *et al.*, *ibid.*, in press.
13. W. F. Bottke Jr. and J. J. Melosh, *Proc. Lunar Planet Sci. Conf.* **26**, 153 (1995).
14. A. W. Harris, *Icarus* **107**, 209 (1994); J. A. Burns and V. S. Safronov, *Mon. Not. R. Astron. Soc.* **165**, 403 (1973).
15. E. Asphaug *et al.*, *Icarus*, in press.

16. Part of this research was conducted at the Jet Propulsion Laboratory, California Institute of Technology, under contract with the National Aeronautics and Space Administration (NASA). Work at Washington State University was supported in part by NASA.

5 May 1995; accepted 14 August 1995

Myt1: A Membrane-Associated Inhibitory Kinase That Phosphorylates Cdc2 on Both Threonine-14 and Tyrosine-15

Paul R. Mueller, Thomas R. Coleman, Akiko Kumagai, William G. Dunphy*

Cdc2 is the cyclin-dependent kinase that controls entry of cells into mitosis. Phosphorylation of Cdc2 on threonine-14 and tyrosine-15 inhibits the activity of the enzyme and prevents premature initiation of mitosis. Although Wee1 has been identified as the kinase that phosphorylates tyrosine-15 in various organisms, the threonine-14–specific kinase has not been isolated. A complementary DNA was cloned from *Xenopus* that encodes Myt1, a member of the Wee1 family that was discovered to phosphorylate Cdc2 efficiently on both threonine-14 and tyrosine-15. Myt1 is a membrane-associated protein that contains a putative transmembrane segment. Immunodepletion studies suggested that Myt1 is the predominant threonine-14–specific kinase in *Xenopus* egg extracts. Myt1 activity is highly regulated during the cell cycle, suggesting that this relative of Wee1 plays a role in mitotic control.

Entry into mitosis is controlled by the M phase–promoting factor (MPF), a complex of the Cdc2 protein kinase and cyclin B. Proper regulation of MPF ensures that mitosis occurs only after earlier phases of the cell cycle have been completed successfully. This strict control of MPF is largely posttranslational, involving the phosphorylation of Cdc2 at three key residues. After Cdc2 associates with cyclin, the cyclin-dependent kinase (CDK)–activating kinase (CAK) phosphorylates Cdc2 on Thr^{161}. This phosphorylation would generate active MPF, but two additional phosphorylations on Thr^{14} and Tyr^{15} of Cdc2 suppress MPF activity during interphase. At the G_2-M transition, the Cdc25 protein dephosphorylates Thr^{14} and Tyr^{15}, thereby allowing MPF to phosphorylate its mitotic substrates (*1*).

Various genetic and biochemical studies have indicated that Wee1 is the kinase that phosphorylates Cdc2 on Tyr^{15}. Wee1 was originally identified in the fission yeast *Schizosaccharomyces pombe* as a critical negative regulator of mitosis (*2*). Subsequently, a second *S. pombe* homolog (Mik1) and Wee1 homologs from at least six other organisms have been found (*3*, *4*). In human and *Xenopus*, Wee1 is a soluble enzyme that phosphorylates Cdc2 on Tyr^{15}, but not on Thr^{14} (*4*–*6*). A Thr^{14}-specific kinase activity has been detected in the membrane fraction of *Xenopus* egg extracts, but the molecular identity of the enzyme has not been established (*7*).

Previously we isolated a *Xenopus* Wee1 homolog. We used degenerate polymerase chain reaction (PCR) primers (based on the sequence similarity between *S. pombe* Wee1, *S. pombe* Mik1, and human Wee1) to amplify a segment of its complementary DNA (cDNA) (*4*). With a different combination of primers, we have amplified a segment of another *Xenopus* oocyte cDNA that appears to encode a distinct member of the Wee1 family. After cloning the corresponding full-length cDNA and characterizing its gene product (Fig. 1A), we designated this protein Myt1 for the membrane-associated, tyrosine- and threonine-specific, Cdc2 inhibitory kinase.

Conceptual translation of the gene encoding Myt1 revealed that it is most similar to kinases in the Wee1 family (Fig. 1B). The kinase domain of Myt1 has a similar degree of sequence similarity with all members of this family, ranging from

Division of Biology 216-76, Howard Hughes Medical Institute, California Institute of Technology, Pasadena, CA 91125, USA.

*To whom correspondence should be addressed.